nature communications

Article

https://doi.org/10.1038/s41467-025-58995-w

TGF-β1-induced m6A modifications accelerate onset of nuclear cataract in high myopia by modulating the PCP pathway

Received: 17 October 2023

Accepted: 9 April 2025

Published online: 24 April 2025

Check for updates

Ling Wei[1,2,3,4,7], Yu Du[1,3,4,7], Shunxiang Gao[5,7], Dan Li[1,3,4], Keke Zhang[1,3,4], Wenwen He[1,3,4], Yi Lu[1,3,4] & Xiangjia Zhu[1,3,4,6]

High myopia is an important cause of visual impairment worldwide, characterized by early-onset nuclear cataracts, whose underlying mechanisms remain largely unexplained. Here, we identify conspicuously polarized and compacted lens fiber alignment, along with a simultaneous rise in N6-methyladenosine (m6A) modifications in patients with highly myopic cataracts (HMC), which is confirmed to be induced by elevated transforming growth factor-β1 (TGF-β1) in lens. Mechanistically, methyltransferase METTL3 and m6A reader insulin-like growth factor 2 mRNA binding protein 3 synergistically enhance planar cell polarity (PCP) signaling by affecting mRNA stability of dishevelled 2. This, in turn, alters proliferation, migration, and polarity formation of human lens epithelial cells. Moreover, Mettl3 conditional knockdown in mice leads to disrupted lens fiber arrangement and alleviates TGF-β1-induced increase in lens nuclear density. Collectively, these findings highlight the significance of m6A-modified PCP pathway in regulating postnatal lens fiber organization, which may hold great promise as a therapeutic target for HMC.

High myopia, characterized by an axial length of 26.00 mm or greater, is becoming a significant concern globally, with an estimated 9.8% of the world population projected to be affected by 2050[1]. This condition increases the risk of multiple oculopathies that can lead to blindness[2]. It is noteworthy that high myopes are reported to develop cataracts at a much earlier age (35–50 years old) and with greater severity compared with non-myopes[3,4]. These cataracts also tend to be of the nuclear type, contrasting the more common cortical opacification observed in age-related cataracts (ARC) among non-myopic individuals[5,6]. Despite these findings, the precise molecular mechanisms underlying the accelerated nuclear sclerosis in highly myopic cataracts (HMC) remain largely unknown.

Highly organized cellular architecture is of utmost importance in maintaining lens transparency. Nevertheless, prior research on cataract pathology has primarily concentrated on lens structural proteins[5,7–10]. In a recent study, we identified dysregulated expression of β/γ-crystallins, resulting in enlarged lenses in HMC[9]. Additionally, we made an intriguing observation that lens fibers in HMC display a striking polarization, with a densely packed nucleus and neatly arranged peripheral fibers resembling the layers of an onion[9]. Whereas, ARC is featured by cohorts of disordered lens fibers located in the cortex. Therefore, we hypothesize the presence of distinct regulatory mechanisms in HMC governing lens fiber alignment, which could potentially contribute to the development of nuclear cataracts.

[1]Department of Ophthalmology, Eye & ENT Hospital, Fudan University, Shanghai, China. [2]Department of Ophthalmology, Sichuan Provincial People's Hospital, Medical School, University of Electronic Science and Technology of China, Chengdu, Sichuan, China. [3]Key Laboratory of Myopia and Related Eye Diseases, NHC; Key Laboratory of Myopia and Related Eye Diseases, Chinese Academy of Medical Sciences, Shanghai, China. [4]Shanghai Key Laboratory of Visual Impairment and Restoration, Shanghai, China. [5]Department of Ophthalmology, Shanghai General Hospital, Shanghai Jiao Tong University School of Medicine, Shanghai, China. [6]State Key Laboratory of Medical Neurobiology, Fudan University, Shanghai, China. [7]These authors contributed equally: Ling Wei, Yu Du, Shunxiang Gao. e-mail: zhuxiangjia1982@126.com

WNT/planar cell polarity (PCP) signaling pathway has been implicated in lens organogenesis. Studies have demonstrated the activation of this signaling cascade following growth factor stimulation, which accounts for the polarization of lens fiber cell during embryonic differentiation[11–14]. However, there is a lack of data regarding the regulation of this pathway in the lens during postnatal development. Recent studies have revealed that N6-methyladenosine (m6A) mRNA modifications confer a critical layer of WNT signaling gene regulation in response to postnatal environmental factors in various diseases[15,16]. Moreover, abnormal m6A modifications induced by growth factors like transforming growth factor-β (TGF-β) have been observed in cells such as retinal epithelial cells and fibroblasts[17–19]. Building upon our previous finding of elevated TGF-β1 in lens epithelial cells (LECs) of highly myopic eyes[9], we propose the possibility that this unique microenvironment may lead to m6A modifications that regulate the alignment of lens fibers by influencing the PCP pathway during the process of HMC formation.

In this vein, we first conducted a series of lens microstructure analyses. As expected, a highly polarized and densely compacted feature of lens fiber alignment in HMC was confirmed. A simultaneous methyltransferase 3 (METTL3)-dependent up-regulation of m6A modifications induced by elevated TGF-β1 in HMC was also identified. Further mechanistic explorations unraveled the cataractogenic role of METTL3 by enhancing PCP signaling through RNA stabilization of disheveled segment polarity protein 2 (DVL2), a crucial PCP component, with insulin-like growth factor 2 mRNA binding protein 3 (IGF2BP3) being the m6A reader. Additionally, in vitro silencing of METTL3 with DVL2 rescue and in vivo conditional knockdown of METTL3 in mouse lens both demonstrated altered LEC proliferation, migration and polarity formation.

Results

Lens fibers in HMC exhibit a highly polarized and compacted property

Clinically, typical ARC mainly manifests as peripheral opacities in the lens cortex, while HMC typically begins in the central nuclear area and rapidly progresses to complete nuclear opacification (Fig. 1a), leading to early visual function impairment. To investigate the microstructure features of HMC, whole-mount lens samples from age-matched donor human cadavers were examined and compared using a freeze-fractured scanning electron microscope (SEM), with a special focus on the juxtanuclear area of the cortex (Fig. 1b). Specifically, lens fibers at the region of interest (ROI) in age-matched clear lens control and HMC demonstrated highly orderly and polarized alignment, whereas in ARC, fibers were disordered with vacuoles and holes commonly seen between fiber conjunctions (Fig. 1c). Notably, lens fibers in HMC were more compacted compared with those in clear lens control and ARC groups (Fig. 1c, d).

To explore the biological behaviors of LECs from ARC and HMC, primary cultures of lens epithelia collected from lens exchange surgery were conducted (Fig. 1e). Compared with those in ARC, the majority of LECs migrating from the rim of the capsule in HMC showed unidirectional orientation with significant cell elongation indicating marked cell polarity (Fig. 1e, f). Meanwhile, the immunofluorescent staining of F-actin also showed that the microfilaments were in a much more paralleled alignment in HMC than in ARC, which was further corroborated quantitatively by further 2-dimensional fast fourier transform (2D FFT) measurement (Fig. 1g and Supplementary Fig. 1).

Together, these results confirm a highly polarized and compacted property of lens fibers and the polarized behavior of LECs in highly myopic eyes, indicating a distinct mechanism underlying early-onset nuclear cataract of highly myopic eyes from the general lens changes of ARC.

TGF-β1 correlates with HMC severity and induces increased m6A modifications in an METTL3-dependent manner

To determine the level of m6A modifications in total RNA, dot blot assays and colorimetric quantification were used, both revealing an elevated abundance of m6A modifications in lens epithelia of HMC compared with those from ARC (Fig. 2a, b). Then, expression patterns of known m6A writers (METTL3, WT1 associated protein [WTAP], and METTL14) and erasers (AlkB Homolog 5, RNA Demethylase [ALKBH5] and FTO alpha-ketoglutarate dependent dioxygenase [FTO]) were screened, and METTL3 was found significantly elevated at both mRNA and protein levels in lens epithelia from HMC (Fig. 2c–e).

Given the unique microenvironment of high myopia, characterized by increased oxidative stress and TGF-β levels[7,9], and the interplay between these factors and m6A modifications in various other diseases[17–19], we re-verified the impaired antioxidant capacity and elevated TGF-β1 signaling in lens epithelia of HMC (Supplementary Fig. 2a–d) and examined their relationship with m6A modifications using human LEC cell line SRA 01/04. Both H_2O_2 and TGF-β1 treatment increased total m6A modifications in LECs (Supplementary Fig. 2e, h). However, only TGF-β1 significantly increased METTL3 expression (Fig. 2f–h) and knockdown or overexpression of METTL3 can decrease or enhance the effect of TGF-β1 on m6A modification (Fig. 2i, j).

Furthermore, the typical cortex opacification of ARC and nuclear opacification of HMC could be distinguished by anterior segment optical coherence tomography (OCT) in vivo (Fig. 2k). A significant correlation was observed between the lens average nucleus density and TGF-β1 concentration in the lens epithelia of HMC patients (Fig. 2k).

Collectively, these results indicate that elevated TGF-β1 in lens of high myopia correlates with HMC nuclear density and may enhance m6A modifications in an METTL3-dependent manner.

METTL3 enhances DVL2-mediated PCP signaling pathway in HMC

In order to obtain a transcriptome-wide m6A map of human LECs, mRNA samples were isolated from lens epithelia of HMC and ARC and were subjected to m6A-modified RNA immunoprecipitation (Me-RIP) followed by sequencing. The m6A modifications were found mostly enriched in the vicinity of coding sequence (CDS) and 3′ untranslated regions (UTR) and the m6A consensus sequence GGAC motif was also identified to be highly enriched within m6A sites in the immunopurified RNA (Fig. 3a–c), which were consistent with previous studies[20,21]. Besides, 981 out of 2335 m6A-modified genes were highly methylated (Fig. 3d, Supplementary Data), with m6A peaks in CDS and 3′UTR higher in HMC (Fig. 3a, b).

We conducted Kyoto Encyclopedia of Genes and Genomes (KEGG) pathway analysis to predict potential pathways associated with m6A modification. Notably, the WNT signaling pathway, known for its indispensable role in lens development, fiber differentiation and cell polarity[11,12,14], was found ranking at the top eight signaling pathway that was potentially affected by m6A modification (Fig. 3e). We thus focused on this pathway and further analyzed the involved genes, among which key transcripts such as WNT3, WNT11, DVL2, etc. were found hypermethylated (Fig. 3f). IGV plots confirmed higher m6A peaks in specific functional regions within WNT3 and WNT11 transcripts in HMC, and the overall distribution of m6A peaks of DVL2 in HMC was significantly higher than ARC (Fig. 3g).

We then compared the expression of key transcripts of WNT signaling identified by the Me-RIP sequencing in lens epithelia of ARC and HMC patients: WNT3 did not show significant difference, while WNT11 and DVL2 were found up-regulated as revealed by qRT-PCR and Western blots (Fig. 4a, b). MeRIP-qPCR further confirmed enhanced m6A modifications of WNT11 and DVL2 transcripts in HMC (Fig. 4c). RIP-qPCR detected that DVL2 mRNA, but not WNT11 mRNA, could be significantly enriched by METTL3-specific antibody compared with the

https://doi.org/10.1038/s41467-025-58995-w

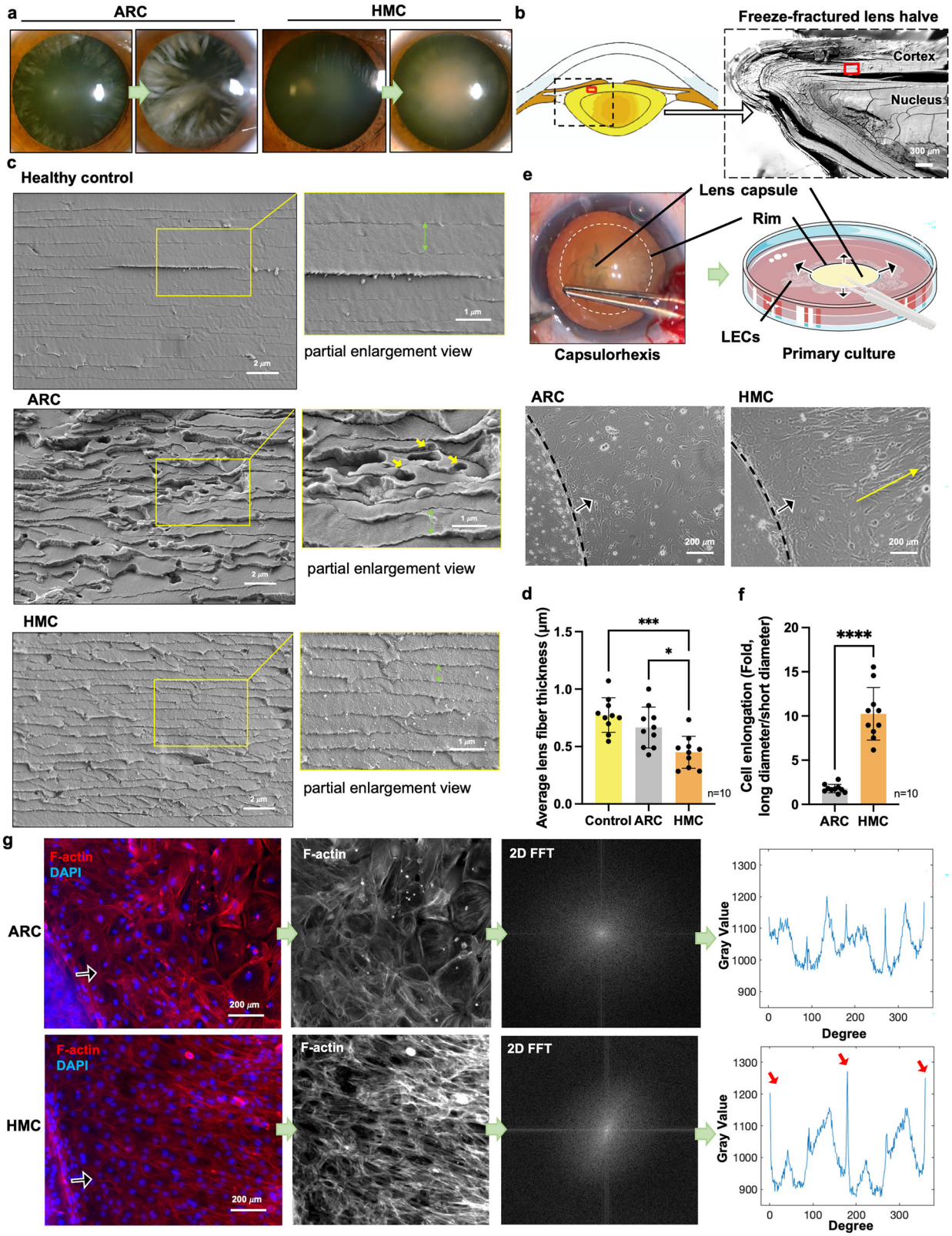

IgG control in SRA 01/04 cells (Fig. 4d), suggesting a direct interaction between METTL3 and DVL2 mRNA. In addition, immunostaining showed that WNT11 was expressed evenly in cytoplasm, while DVL2 was expressed asymmetrically in LECs from HMC patients forming a polarized pattern (Fig. 4e). Given that the HMC group did not demonstrate enhanced β-catenin stability but showed significant up-regulation in phospho-Jun N-terminal kinase (p-JNK) protein (Fig. 4f; Supplementary Fig. 3a), the noncanonical PCP/p-JNK signaling pathway might have been activated by abundant m6A modifications in HMC.

Based on the above-mentioned evidence, we knew that PCP signaling was possibly boosted by METTL3 in HMC. Overexpression of METTL3 increased DVL2 expression but not WNT11 (Fig. 4g, h; Supplementary Fig. 3b), and boosted the expression of p-JNK, the

Fig. 1 | The lens fibers of human highly myopic cataracts exhibit a highly polarized and compacted alignment. a Representative slit-lamp photos of cataract (mild to severe) from typical human ARC and HMC eyes. **b** The schematic diagram of human lens (left) and an example SEM pre-scan of the human donor freeze-fractured lens half (Right, scale bar: 300 μm). Red rectangles show the ROI at the juxtanuclear area of the cortex in formal scans. **c** Representative freeze-fractured SEM scans of lens fibers in ROIs with enlarged views from age-matched healthy controls, ARC, and HMC lenses. Yellow rectangles highlight enlarged areas; yellow arrows indicate vacuoles/holes in fiber junctions; green arrows show fiber thickness. Scale bar: 2 μm (formal scan), 1 μm (enlarged view). **d** The average lens fiber thickness in control, ARC, and HMC measured in SEM scans ($n = 10$, control: ARC: $p = 0.0002$, HMC: $p = 0.0129$). **e** Schematic of primary human LEC culture. After capsulorhexis during cataract surgery, the lens capsule was collected and adhered to Petri dishes, allowing LECs to proliferate and migrate from the capsule rim (black arrows). Representative images show distinct LEC phenotypes from ARC and HMC patients. Dotted lines mark the capsule rim; black arrows show migration direction; yellow arrow indicates cell polarity. Scale bar: 200 μm. **f** Ratio of longest to shortest axis in migrated LECs compared between ARC and HMC; $n = 10$, $p < 0.0001$. **g** The immunofluorescent staining of F-actin in primary culture of human ARC and HMC LECs. Scale bar: 200 μm. The 2D FFT was conducted to obtain quantitative data of cell alignment. Radial sums were taken over the 2D FFT from 0° to 360° and plotted as raw intensity (gray value) vs. angle (degree). Red arrows show the intensity peaks in 0°, 180°, and 360° were evident for aligned cells (from HMC) but less so for random cells (from ARC). n = biological replicates. Data present are mean ± SD. Level of significance was detected using one-way ANOVA (**d**) and unpaired two-sided Student's t-test (**f**). $^{****}p < 0.0001$, $^{***}p < 0.001$, $^{*}p < 0.05$.

downstream mediator of PCP pathway (Fig. 4i and Supplementary Fig. 3c) in SRA 01/04 cells. Conversely, METTL3 knockdown by siRNA decreased DVL2 and p-JNK expression (Fig. 4j and Supplementary Fig. 3d, e). MERIP-qPCR results indicated enhanced m6A modifications of the DVL2 mRNA upon METTL3 overexpression and reduced modifications after METTL3 knockdown (Fig. 4k, l).

These findings are all supportive of the fact that METTL3-induced m6A modifications target at DVL2-mediated PCP signaling pathway in HMC.

DVL2 RNA is stabilized by IGF2BP3 via reading m6A modification in HMC

To identify the m6A reader protein potentially responsible for m6A-induced DVL2 regulation in HMC, we tested the expression of known readers in human lens epithelia, including YTHDF1, YTHDF2, YTHDC1, and IGF2BP1/2/3, and found that IGF2BP3 and YTHDF2 expression were elevated in HMC (Fig. 5a, b). Considering that DVL2 is an established target of IGF2BP3 rather than YTHDF2, as reported in previous studies by high-throughput RIP-sequencing[22,23], we focused our further explorations on IGF2BP3 and confirmed a decreased DVL2 expression after IGF2BP3 knockdown in SRA 01/04 cells (Fig. 5c, d). RIP-qPCR detected that DVL2 mRNA could be significantly enriched by IGF2BP3-specific antibody compared with the IgG control and more importantly, this interaction could be disrupted by METTL3 deficiency (Fig. 5e).

To further explore whether IGF2BP3 affected DVL2 expression via regulation of mRNA stability, mRNA levels were detected after the treatment of actinomycin D, a transcription inhibitor. The half-life of DVL2 mRNA could be significantly shortened after IGF2BP3 and METTL3 knockdown, respectively (Fig. 5f). Taken together, our data suggest that the m6A writer METTL3-mediated methylation of DVL2 transcripts can be directly recognized by the m6A reader, IGF2BP3, and thus maintain the stability of the transcripts and increase its expression in HMC.

M6A-modified DVL2 promotes proliferation, migration, and polarity formation of LECs

The investigation into functional significance of TGF-β1-m6A-DVL2 axis in regulating LECs was conducted. In SRA 01/04 cells, knockdown of METTL3 and IGF2BP3 down-regulated TGF-β1-induced DVL2/p-JNK overexpression (Fig. 6a, b), as well as inhibited cell proliferation (Fig. 6c) and migration (Fig. 6d).

Since the DVL2-mediated PCP signaling pathway is recognized as part of fibroblast growth factor 2 (FGF-2) induced cascade that promotes lens fiber differentiation[12], we adopted FGF-2 as the stimulator of DVL2. FGF-2 alone elevated DVL2 expression and enhanced proliferation and migration of SRA 01/04 cells, which could be reversed by the treatment of an established DVL2 inhibitor, IWP-2 (Fig. 6e–h, and Supplementary Fig. 4a). In addition, FGF-2 treatment of primary cultured LECs from ARC patients resulted in more significant cell elongation and polarity with actin filaments becoming more isotropic and paralleled to the long axis (Fig. 6i, j and Supplementary Fig. 4b), suggesting that the overexpression of DVL2 could promote cytoskeletal rearrangement and polarity formation.

Furthermore, SRA 01/04 cells were subjected to different combinations of METTL3 knockdown, DVL2 overexpression, FGF-2 and IWP-2 treatment. METTL3 knockdown-induced down-regulation of DVL2 and downstream p-JNK in PCP signaling pathway could be rescued by both FGF-2 treatment and DVL2 overexpression, whereas the addition of IWP-2 further suppressed the rescue effect of FGF-2 (Fig. 6k, l). METTL3 knockdown could also inhibit cell proliferation and migration, both of which could be reversed by FGF-2 treatment or DVL2 overexpression as shown by CCK-8 and wound healing assay (Fig. 6m, n).

These findings together suggest that the METTL3-mediated m6A modifications of DVL2 play a crucial role in regulating PCP pathway and in promoting cell proliferation, migration, and polarity formation of LECs.

Lens-specific knockdown of Mettl3 leads to mitigation of TGF-β1-induced increase of fiber compaction and nuclear intensity

To reveal the role of METTL3-DVL2 axis in lens fiber alignment in vivo, lens-specific *Mettl3* conditional knockdown mice were generated using the Cre/LoxP system. *Prox1-CreERT*$^{ct2/wt}$*;Mettl3*$^{flox/flox}$ mice (cKD) were treated with tamoxifen to induce expression of the Cre transgene[24], and *Prox1-CreERT*$^{wt/wt}$*;Mettl3*$^{flox/flox}$ mice (WT) were used as controls. Down-regulation of METTL3, DVL2, and p-JNK were all verified in lens epithelia of cKD mice (Fig. 7a, b). Wheat germ agglutinin (WGA) immunostaining displayed different membrane morphologies of secondary fiber cells in the juxtanuclear areas at the equator of the lens (where LECs proliferate and differentiate into new fibers that are progressively added to the cortex and nucleus[25]), of which lens fibers in WT mice were well-organized and aligned whereas those in cKD mice were disordered and discontinuous (Fig. 7c). SEM scans of secondary fiber cells also showed disarray in cKD mice (Fig. 7d). These suggest that METTL3 may play an important role in alignment and formation of secondary lens fibers.

In addition, we performed intravitreal injections of active TGF-β1 in WT and *Mettl3* cKD mice to replicate the TGF-β1-abundant microenvironment typically observed in HMC patients (Fig. 7e). Two weeks after injection, though slit-lamp images showed no significant nuclear cataract formation (Supplementary Fig. 5), lens fiber compaction was confirmed by SEM scans (Fig. 7f), and the compaction was less pronounced in *Mettl3* cKD mice. OCT images further showed a significant increase in lens nuclear intensity in WT mice (Fig. 7g), which was less prominent in *Mettl3* cKD mice (Fig. 7f, g).

Overall, these findings suggest that lens-specific conditional knockdown of METTL3 in mice may down-regulate the DVL2-dominated PCP signaling pathway, leading to disordered lens fiber alignment in secondary lens fiber cells. Additionally, METTL3 knockdown may reduce the TGF-β1-induced increase in lens fiber compaction and nuclear intensity.

https://doi.org/10.1038/s41467-025-58995-w

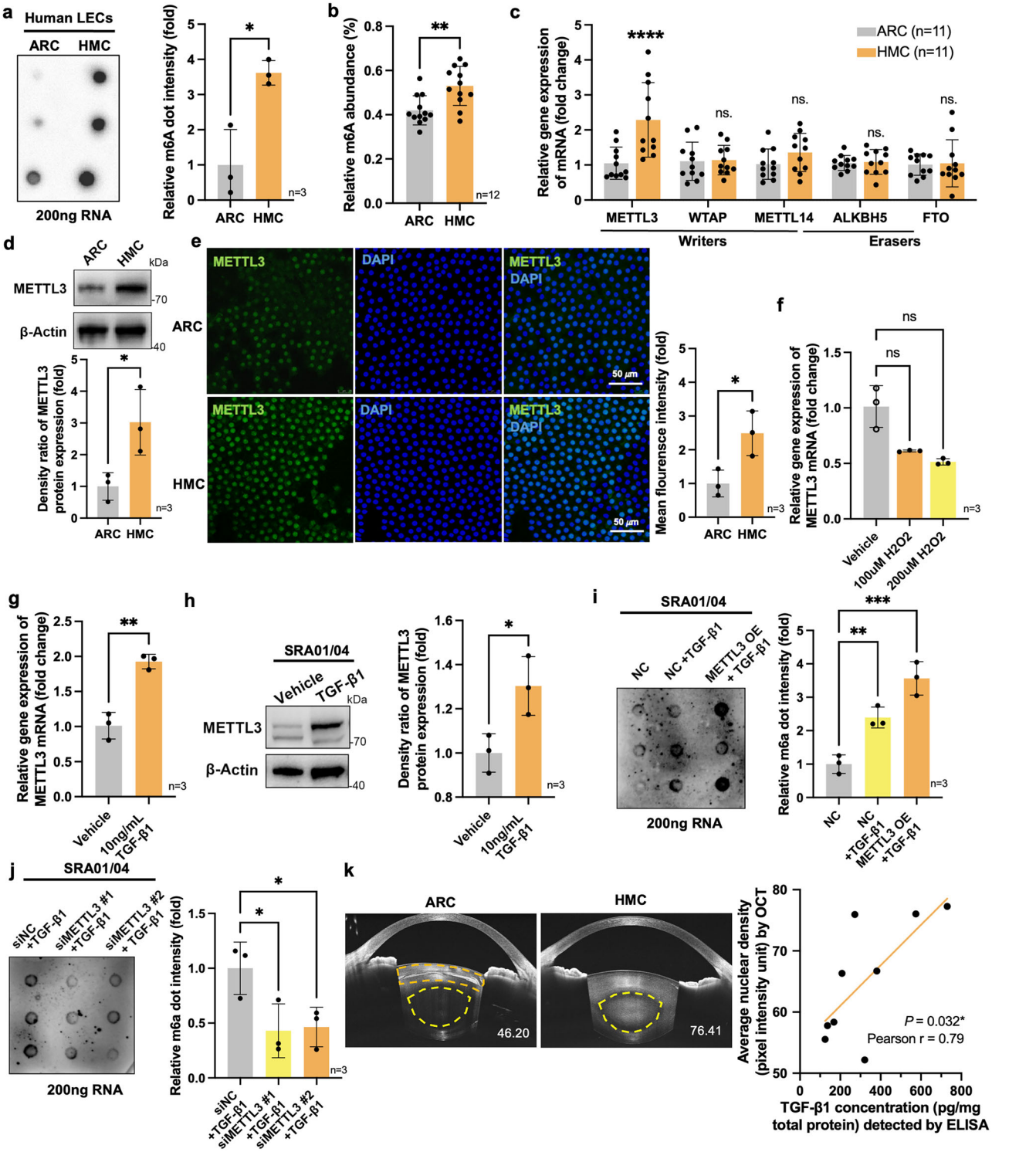

Fig. 2 | TGF-β1 correlates with HMC severity and induces increased m6A modifications in an METTL3-dependent manner. a The dot blot assay of m6A abundance ($n = 3$, $p = 0.0130$). **b** Colorimetric quantification of relative m6A abundance ($n = 12$, $p = 0.0022$). **c** Gene expressions of m6a writers ($n = 12$, METTL3 $p < 0.0001$, WTAP $p > 0.9999$, METTL14 $p = 0.5750$, ALKBH5 $p > 0.9999$, and FTO $p > 0.9999$). **d** METTL3 protein expression in ARC and HMC ($n = 3$, $p = 0.0352$). **e** Nuclear staining of METTL3 in ARC and HMC ($n = 3$, $p = 0.0290$). The nuclear counter stain is DAPI. Scale bar: 50 μm. **f** METTL3 gene expression in cells treated with vehicle, 100 μM or 200 μM H_2O_2 ($n = 3$, 100 μM $p = 0.0945$, 200 μM $p = 0.0570$). **g** METTL3 gene expression in cells treated with vehicle or 10 ng mL^{-1} TGF-β1. ($n = 3$, $p = 0.0345$) **h** METTL3 protein expression in cells treated with vehicle or 10 ng mL^{-1} TGF-β1 ($n = 3$, $p = 0.0297$). **i, j** The dot blot assay of m6A abundance in cells with defferent treatments. ($n = 3$, **i**: NC + TGF-β1 $p = 0.0072$, METTL3 OE + TGF-β1, $p = 0.0003$; **j**: NC + TGF-β1 $p = 0.0360$, METTL3 OE + TGF-β1 $p = 0.0456$). **k** Preoperative anterior segment OCT images of lenses from ARC and HMC patients. Orange and yellow dotted circles indicate the cortex and nucleus, respectively. Average nuclear intensity was noted at bottom right. Correlation between preoperative nuclear intensity and their LEC TGF-β1 concentrations is shown. ($n = 9$, $p = 0.0318$). The band or dot density was normalized to loading control as a ratio for statistical analysis. Data present are mean ± SD. Level of significance was detected using two-sided Student's *t* test (**a**, **b**, **d**, **e**, **g**, **h**), one-way ANOVA with Dunnett's multiple comparisons test (**f**, **i**, **j**), two-way ANOVA with Šídák's multiple comparisons test (**c**), and Pearson's correlation analysis (**k**). *n* = biological replicates, ns. = not significant, $^{****}p < 0.0001$, $^{***}p < 0.001$, $^{**}p < 0.01$ and $^{*}p < 0.05$.

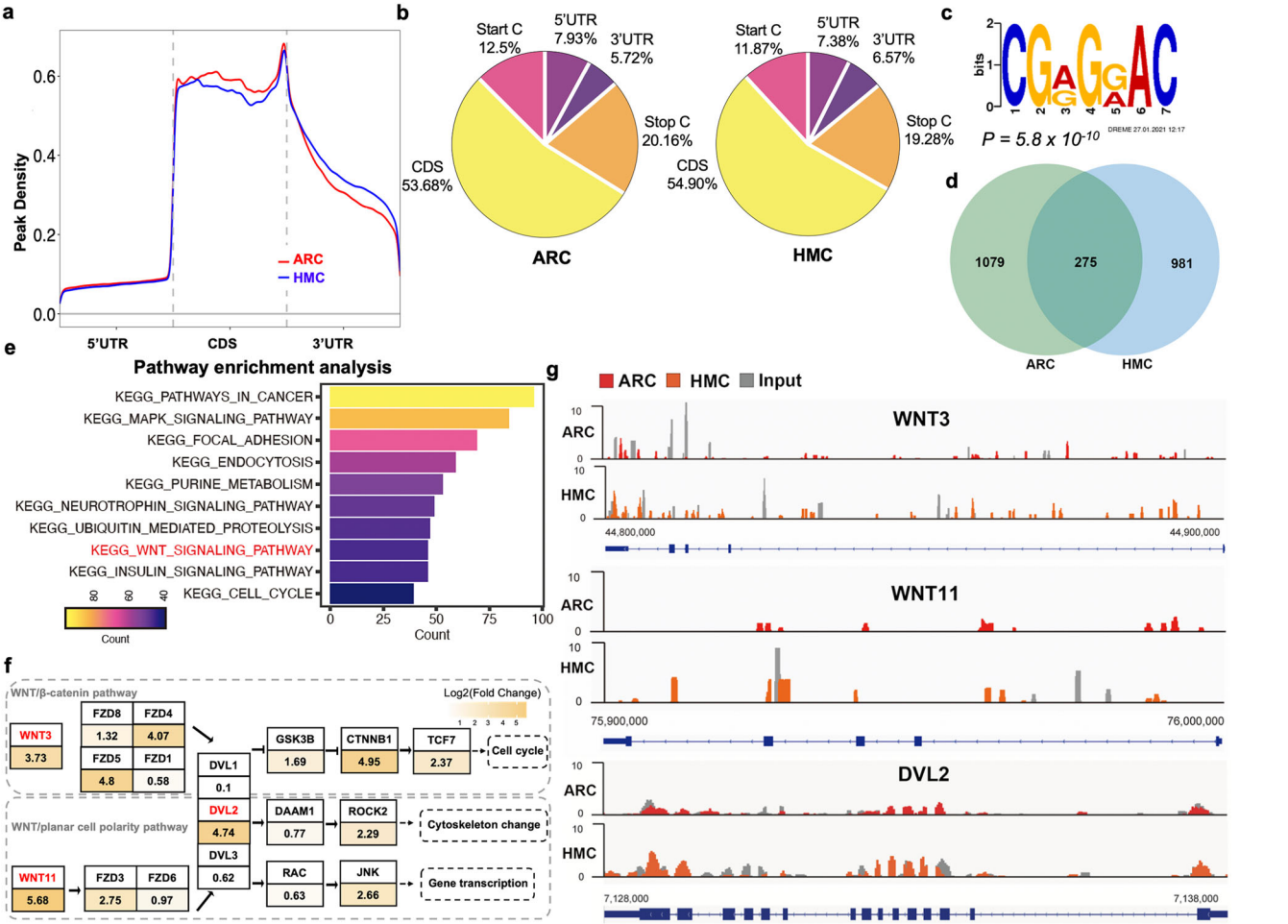

Fig. 3 | High-throughput m6A-sequence profiling of lens epithelial tissues from HMC and ARC patients. a The normalized distribution of m6A peaks across the start codon, coding sequence, stop codon of mRNAs in lens epithelia of age-related cataract (ARC) and highly myopic cataract (HMC) patients. **b** The pie graphs of m6A peak distribution showing the proportion of total m6A peaks in the indicated regions of mRNAs in lens epithelia of ARC and HMC. **c** Top consensus motif identified by DREME with m6A-seq in lens epithelia. Fisher's Exact Test p = 5.8e-10. **d** Venn diagrams showing the overlapping and differentially m6A modified genes expressed in lens epithelia of ARC and HMC. **e** KEGG pathway analysis of transcripts with increased m6A methylation in lens epithelia of HMC compared with ARC. The diagram is based on KEGG annotations with the numbers of m6A-modification up-regulated peaks per the color gradient shown. **f** KEGG annotated diagram of the WNT signaling pathways with genes affected by m6A modification. Log2(fold change) was noted in HMC compared with ARC. **g** The IGV plots showing the m6A abundances in WNT3, WNT11, and DVL2 in lens epithelia of HMC compared with ARC.

Discussion

High myopia is a complicated ocular disorder that is associated with various ocular comorbidities and can lead to blindness. In particular, cataracts in high myopia, being the most commonly seen complications of high myopia, feature early onset and typical nuclear sclerosis, rapid progression and poor prognosis, which causes significant concern[5,6]. An obstacle to effectively intervening in presenile nuclear sclerosis of HMC is the incomplete understanding of its underlying mechanism, particularly regarding fiber alignment, in addition to previously recognized alternations in structural proteins[5,7,8]. Herein, we demonstrated that the fiber alignment of highly myopic lens exhibited a highly polarized and compacted property compared with ARC or clear lens. We also observed a significant increase in m6A levels in the lens, mediated by TGF-β1, which positively correlated with HMC severity. This was accompanied by up-regulation of METTL3, enhancing m6A modifications of DVL2 mRNA and stabilizing it through m6A reader IGF2BP3. The m6A-modified DVL2 subsequently promoted PCP/p-JNK signaling pathway, leading to enhanced cell proliferation, migration, polarity formation, and organized lens fiber alignment in HMC. Collectively, our study uncovers a previously unrecognized role for TGF-β1-induced m6A modifications in accelerating nuclear cataractogenesis in high myopia through PCP signaling pathway.

In contrast to the disorder in fiber arrays of typical cortical opacifications in ARC, the lens fiber alignment in HMC displays a markedly polarized and organized property at both macroscopic and microscopic levels, which could not be fully explained by the altered expressions or modifications of crystallin proteins as indicated by previous studies[9,10,26–28]. During vertebrate gastrulation, the eye lens develops a polarized structure through the highly coordinated behavior of its cells[12,14,29]. LECs proliferate and migrate at the lens equator and differentiate into secondary lens fibers, which continues throughout life[11,14,30]. With aging, the lens undergoes continuous fiber differentiation and accretion, resulting in increased fiber compaction. This compaction has been recognized as a senescent alteration of the lens, contributing to the formation of nuclear cataracts[31]. In a previous study, we reported that in highly myopic lens, β/γ-crystallin expressions were abnormally elevated, leading to enlarged lens size[9,10,28]. Further in this study, we found significant cell proliferation, migration, polarity formation, and cytoskeleton reorganization in LECs from HMC patients. These factors may be driving factors for the accelerated concentric compression of lens fibers, indicating that in high myopia,

https://doi.org/10.1038/s41467-025-58995-w

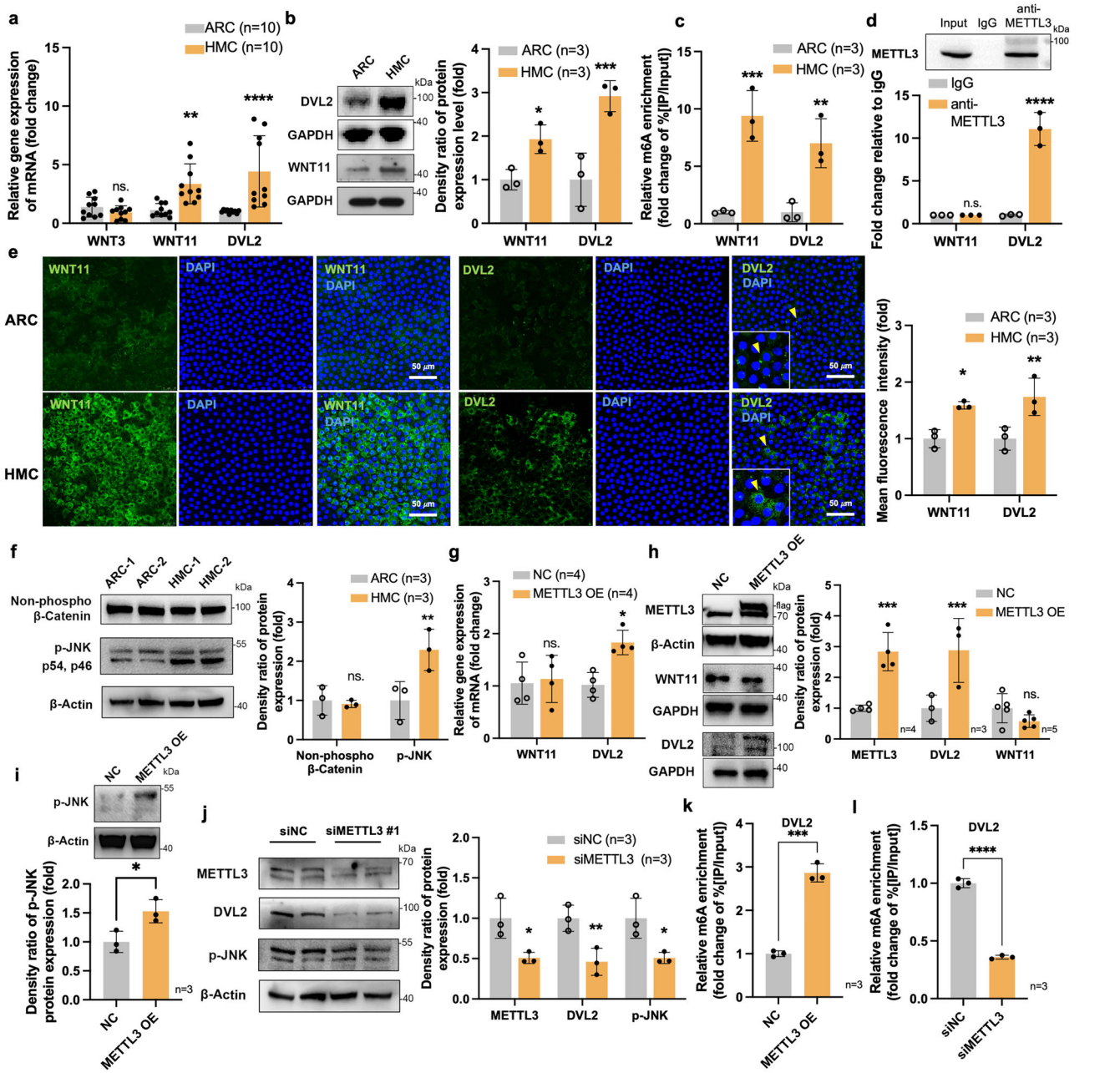

Fig. 4 | DVL2-mediated PCP signaling pathway is the target of METTL3 in HMC. **a** Gene expressions in ARC and HMC ($n = 10$, WNT3 $p = 0.8708$, WNT11 $p = 0.0046$ and DVL2 $p < 0.0001$). **b** Protein expressions in ARC and HMC ($n = 3$, WNT11 $p = 0.0464$, DVL2 $p = 0.0008$). **c** The m6A modification levels in ARC and HMC ($n = 3$, WNT11 $p = 0.0004$, DVL2 $p = 0.0034$). **d** Upper: Western blot of co-precipitated proteins in endogenous METTL3 RIP analysis. Lower: qRT-PCR of co-precipitated mRNAs using METTL3 antibody in SRA 01/04 cell RIP analysis. IgG served as isotype control. ($n = 3$, WNT11 $p > 0.9999$, DVL2 $p < 0.0001$). **e** The immunofluorescent staining of WNT11 and DVL2 in ARC and HMC ($n = 3$, WNT11 $p = 0.0187$, DVL2 $p = 0.0056$). Yellow arrows indicate the enlarged view of DVL2's polarized localization. Scale bar: 50 μm. **f** Protein expressions in ARC and HMC ($n = 3$, β-catenin $p = 0.9594$, p-JNK $p = 0.0091$). **g** Gene expressions in METTL3 OE cells ($n = 4$, WNT11 $p = 0.9346$, DVL2 $p = 0.0121$). NC = negative control. **h** Protein expressions in METTL3 OE cells (METTL3: $n = 4$, $p = 0.0003$; DVL2: $n = 3$, $p = 0.0009$; WNT11: $n = 5$, $p = 0.5131$). **i** p-JNK protein expressions in METTL3 OE cells ($n = 3$, $p = 0.0281$). **j** Protein expressions in cells transfected with siMETTL3 #1 ($n = 3$, METTL3 $p = 0.0153$, DVL2 $p = 0.0084$, p-JNK $p = 0.0153$). The m6A modification levels of DVL2 mRNA in METTL3 OE (**k**) or siMETTL3 (**l**) cells ($n = 3$, **k**: METTL3 OE $p = 0.0001$; **l**: siMETTL3 $p < 0.0001$). Data present are mean ± SD. The band density in Western blot was normalized to loading control as a ratio for statistical analysis. Level of significance was detected using two-sided Student's t test (**i**, **k**, **l**) or two-way ANOVA with Šídák's multiple comparisons test (**a**–**h**, **j**). n = biological replicates, ns. = not significant, $^{****}p < 0.0001$, $^{***}p < 0.001$, $^{**}p < 0.01$ and $^{*}p < 0.05$.

aging process of lens have been somehow aberrantly activated, leading to accelerating lens fiber differentiation and passive inward compression. Whereas in most ARC cases, the aging process gradually manifests as disarray and vacuoles in cortical areas of the lens[32,33].

Extensive research has been conducted on the regulation of lens fiber differentiation and orientation during embryonic development[12,14,29], yet the exploration of postnatal variations has been largely overlooked. Generally, this process cannot be divorced from impacts of growth factors[26,27,34]. Interestingly, TGF-β1 has been identified as an upstream regulator of aberrant lens growth in highly myopic patients according to one of our previous studies[9]. However, there is no ready answer to how it might have participated in the lens fiber

https://doi.org/10.1038/s41467-025-58995-w

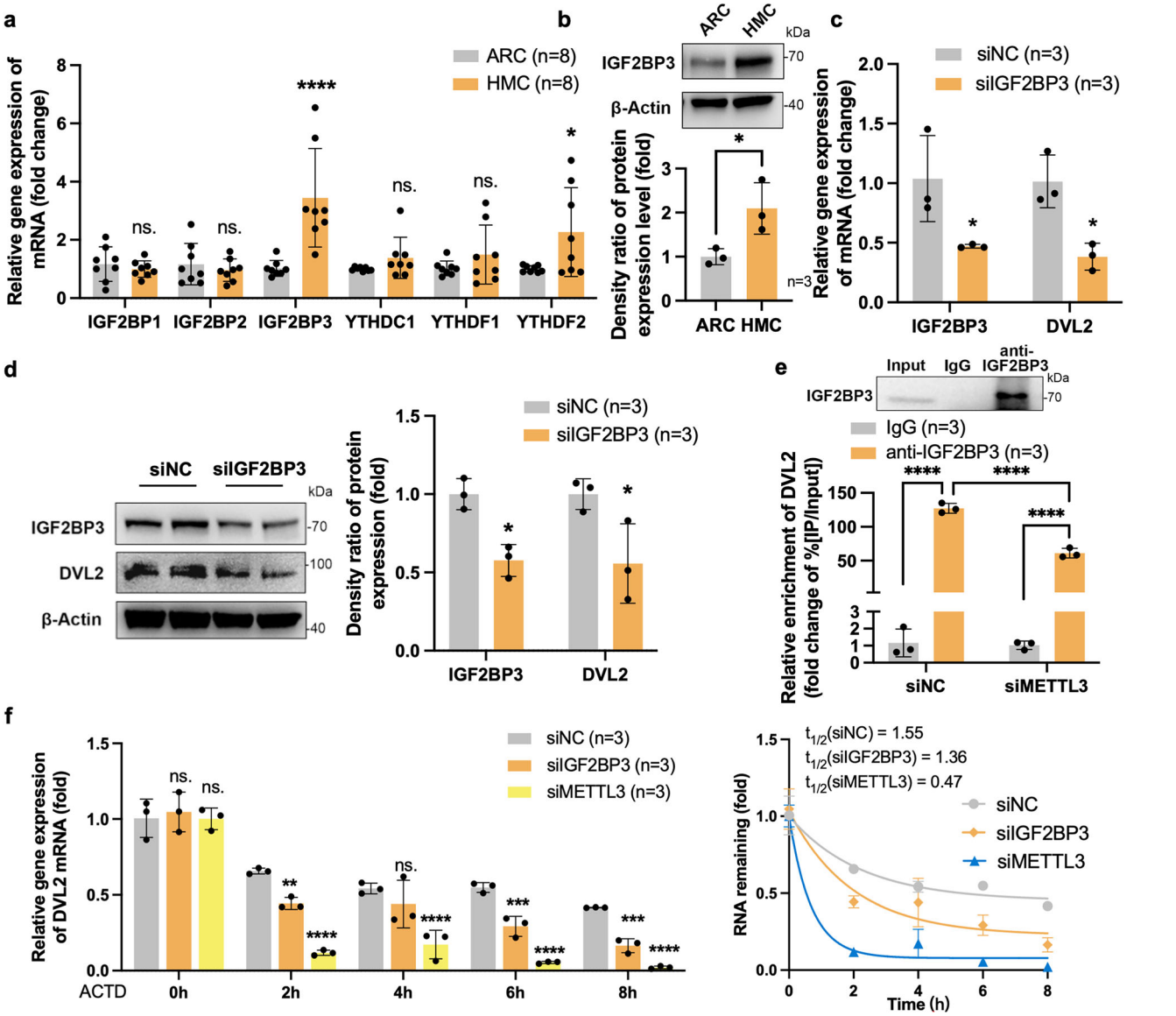

Fig. 5 | The m6A-modified DVL2 mRNA is stabilized by IGF2BP3 in LECs of HMC. **a** Gene expressions of m6A readers in ARC and HMC ($n = 8$, IGF2BP1 $p = 0.9988$, IGF2BP2 $p = 0.9972$, IGF2BP3 $p < 0.0001$, YTHDC1 $p = 0.9271$, YTHDF1 $p = 0.8213$, YTHDF2 $p = 0.0155$). **b** IGF2BP3 protein expression in ARC and HMC ($n = 3$, $p = 0.0363$). The genes (**c**) and protein (**d**) expressions in cells treated with IGF2BP3 siRNA ($n = 3$, **c**: IGF2BP3 $p = 0.0260$, DVL2 $p = 0.0153$, **d**: IGF2BP3 $p = 0.0193$, DVL2 $p = 0.0154$). **e** Upper: Co-precipitated proteins in endogenous IGF2BP3 RIP analysis. Lower: Co-precipitated DVL2 mRNAs by IGF2BP3 antibody in RIP analysis of cells transfected with siNC or siMETTL3 #1. IgG served as the isotype control. ($n = 3$, all $p < 0.0001$). **f** RNA stability test. Left: The DVL2 gene expressions in each time point ($n = 3$, 0 h: siMETTL3 $p = 0.9972$, siIGF2BP3 $p = 0.7163$; 2 h: siMETTL3 $p < 0.0001$, siIGF2BP3 $p = 0.0026$; 4 h: siMETTL3 $p < 0.0001$, siIGF2BP3 $p = 0.1751$; 6 h: siMETTL3 $p < 0.0001$, siIGF2BP3 $p = 0.0004$; 8 h: siMETTL3 $p < 0.0001$, siIGF2BP3 $p = 0.0005$). Right: Lifespans of DVL2 mRNA. Data present are mean ± SD. The band density was normalized to loading control as a ratio for statistical analysis. Level of significance was detected using two-sided two-way ANOVA with Šídák's multiple comparisons test (**a**, **c**–**f**) and unpaired Students' *t* test (**b**). *n* = biological replicates, ns. = not significant, $^{****}p < 0.0001$ $^{***}p < 0.001$, $^{**}p < 0.01$ and $^{*}p < 0.05$.

alignment. In this study, we further examined and confirmed its positive association with lens density in HMC. Considering that the lens differences between highly myopic eyes and normal eyes are not likely to be innate, mechanisms mediating long-term and chronic impacts on lens in response to gradually excessive axial elongation and altered intraocular microenvironment such as epigenetic modifications seem reasonable to be a link between TGF-β1 and the accelerated condense of lens nucleus.

Our data do suggest that TGF-β1 increases the level of RNA m6A modifications in HMC. Although TGF-β1 may also act as an EMT inducer that transforms primary LECs into myofibroblast cells[35], our initial investigation revealed no elevation in the EMT process in HMC (Supplementary Fig. 6). This suggests that the EMT process is unlikely to be promoted by TGF-β1 in the pathogenesis of HMC. Instead, TGF-β1 might have influenced the specific arrangement and compaction of lens fibers through alternative pathways. m6A modifications, being the most prevalent modification in eukaryotic mRNA, plays a crucial role in regulating gene expression by influencing mRNA stability, translation, and alternative splicing[22,36,37]. The dynamic regulation of m6A modifications has been associated with various biological processes, including angiogenesis[38], etc. We found that elevated TGF-β1 coincided with increased m6A modifications as well as up-regulation of m6A writer, METTL3, the latter two of which were replicated in human LEC cell line after TGF-β1 treatment. Similar interplays between TGF-β1

https://doi.org/10.1038/s41467-025-58995-w

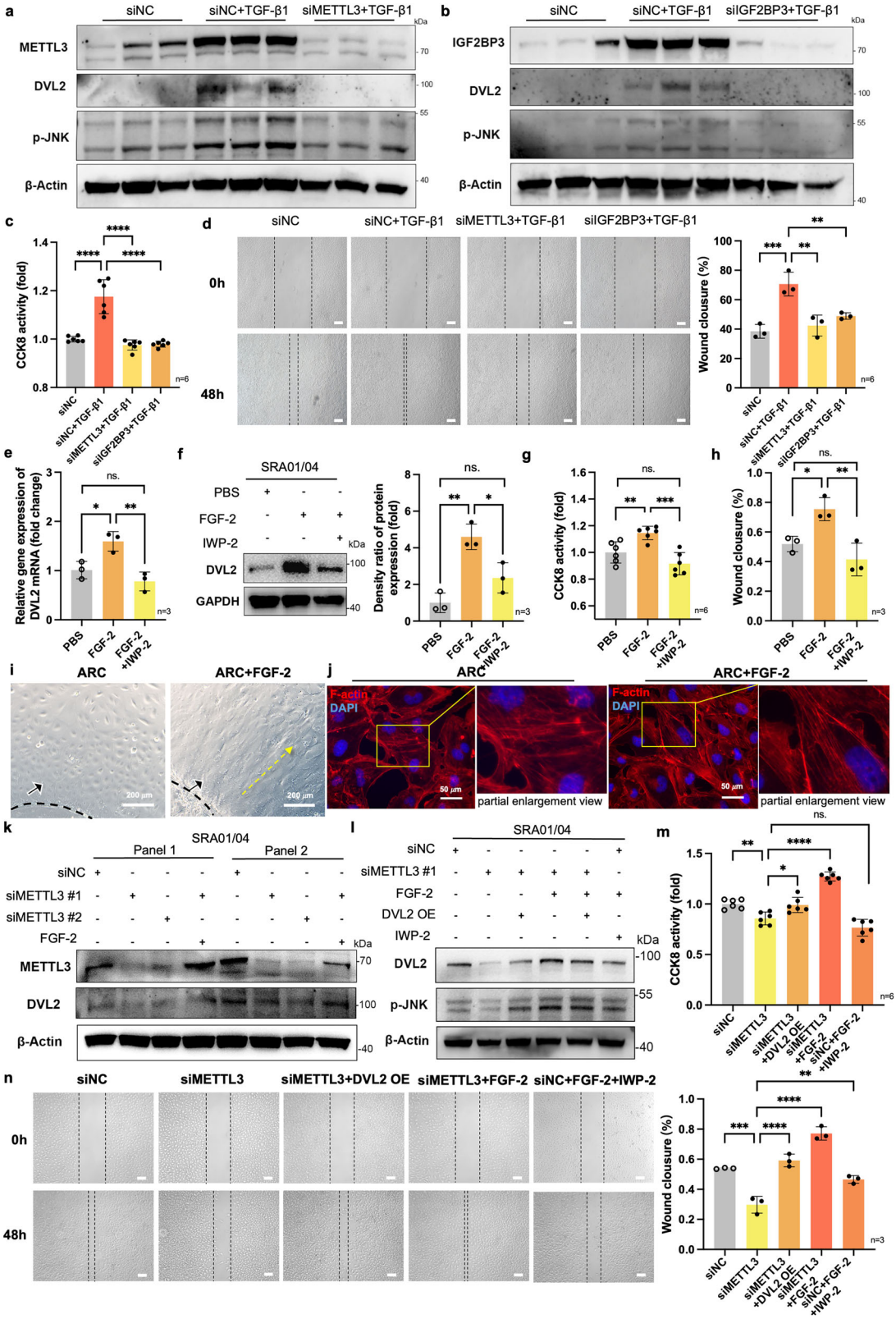

and METTL3 have been reported in excessive human Tenon's capsule fibroblast activation after glaucoma filtration surgery[18].

Pathway analysis of high-throughput m6A sequencing in HMC and ARC lens epithelia identified the WNT signaling pathway. Although other pathways, such as ubiquitination, are also crucial in cataract research, particularly for crystallin modifications and degradation[39], we focused on the WNT pathway due to its key role in lens fiber alignment. Further investigations focused on the non-canonical PCP signaling pathway, represented by WNT11 and DVL2, whose expressions were found significantly elevated in the lens epithelia of HMC. Yet, only DVL2 was confirmed to have direct interaction with METTL3. DVL2, being an essential component of non-canonical PCP pathway, exhibited high levels of mRNA methylation with expression up-regulation in HMC and a polarized distribution in the cytoplasm.

Fig. 6 | The m6A modifications of DVL2 promote cell proliferation, migration, and polarity formation in LECs of HMC. a, **b** Protein expressions in cells with different treatments. Cell proliferation (**c**) and migration (**d**) in cells with different treatments ($n = 6$, **c**: siNC vs. siNC+TGF-β1 $p < 0.0001$, siNC+TGF-β1 vs. siMETTL3+TGF-β1 $p < 0.0001$, siNC+TGF-β1 vs. siIGF2BP3+TGF-β1 $p < 0.0001$; **d**: siNC vs. siNC+TGF-β1 $p = 0.0006$, siNC+TGF-β1 vs. siMETTL3+TGF-β1 $p = 0.0015$, siNC+TGF-β1 vs. siIGF2BP3+TGF-β1 $p = 0.0073$;). Scale bar: 100 μm. **e** DVL2 gene expression in cells with different treatments ($n = 3$, PBS vs. FGF-2 $p = 0.0215$, PBS vs. FGF-2 + IWP-2 $p = 0.3595$, FGF-2 vs. FGF-2 + IWP-2 $p = 0.0045$). **f** DVL2 protein expression in cells with different treatments ($n = 3$, PBS vs. FGF-2 $p = 0.0018$, PBS vs. FGF-2 + IWP-2 $p = 0.1168$, FGF-2 vs. FGF-2 + IWP-2 $p = 0.0178$). Cell proliferation (**g**) and migration (**h**) of cells with different treatments ($n = 3$; **g**: PBS vs. FGF-2 $p = 0.0089$, PBS vs. FGF-2 + IWP-2 $p = 0.1451$, FGF-2 vs. FGF-2 + IWP-2 $p = 0.0002$; **h**: PBS vs. FGF-2 $p = 0.0319$, PBS vs. FGF-2 + IWP-2 $p = 0.3418$, FGF-2 vs. FGF-2 + IWP-2 $p = 0.0060$). **i** Primary culture of ARC with FGF-2. Scale bar: 200 μm. Black arrows indicate the original capsule rim; yellow arrow shows cell polarity direction. **j** Immunofluorescent staining in primary cultures of ARC with FGF-2. Scale bar: 20 μm. **k**, **l** Protein expression in cells with different treatments. Cell proliferation (**m**) and migration (**n**) in cells with different treatments ($n = 6$, **m**: siNC vs. siMETTL3 $p = 0.0060$, siMETTL3 vs. siMETTL3 + DVL2 OE $p = 0.0114$, siMETTL3 vs. siMETTL3 +FGF−2 $p < 0.0001$, siMETTL3 vs. siNC+FGF-2 + IWP-2 $p = 0.1302$; **n**: siNC vs. siMETTL3 $p = 0.0001$, siMETTL3 vs. siMETTL3 + DVL2 OE $p < 0.0001$, siMETTL3 vs. siMETTL3 +FGF-2 $p < 0.0001$, siMETTL3 vs. siNC+FGF-2 + IWP-2 $p = 0.0024$). Scale bar: 50 μm.The band density was normalized to loading control as a ratio for statistical analysis. Level of significance was detected using two-sided one-way ANOVA with Tukey's multiple comparisons test (**c**–**h**, **m**, **n**). n = biological replicates, ns. = not significant, $^{****}p < 0.0001$, $^{***}p < 0.001$, $^{**}p < 0.01$ and $^{*}p < 0.05$.

While the role of DVL2-mediated PCP signaling pathway in embryonic lens development and fiber differentiation is well-established[12,13,40], its impact on the mature lens during aging remains unexplored. Our findings, combined with previous observations of increased secondary lens fiber layers in highly myopic eyes[9], support the hypothesis that METTL3-induced m6A modifications target at DVL2-mediated PCP signaling pathway. This aberrant activation of signaling may lead to persistent LEC proliferation and lens fiber differentiation, ultimately resulting in accelerated concentric compressions of lens fibers and the onset of nuclear sclerosis.

Additionally, our findings indicate that following m6A modification, the mRNA of DVL2 was recognized and stabilized by the m6A reader IGF2BP3. METTL3 deficiency decreased stability of DVL2 transcripts in SRA 01/04 cells, which can be attributed to the reduced m6A modifications that are preferentially recognized and bound by IGF2BP3. A recent study has discovered the ability of IGF2BPs to identify m6A modifications and their crucial role in enhancing the stability and translation of numerous mRNA transcript. Through high-throughput sequencing analyses, DVL2 has been identified as one of the targets of IGF2BP2 and IGF2BP3[22]. IGF2BPs were previously found to be regulating key transcripts of aging and anti-tumor immunity[20,41–43]. Our results firstly confirm that IGF2BP3 selectively recognizes m6A-modified DVL2 mRNA and promotes mRNA stability. In future research, measuring translation efficiency and investigating the potential role of other m6A readers might also be crucial for a comprehensive understanding the regulatory roles of m6A in lens biology.

We then demonstrated the role of PCP/p-JNK signaling pathway in regulating the proliferation, migration, and polarity formation in LECs and thus lead to distinct morphological features of highly-polarized fiber alignment in highly myopic lens. The process of oriented cell migration and polarity relies on the presence of asymmetric cues, such as FGF-2[12], which triggers the reorganization of the cytoskeleton and the polarized localization of important proteins[14]that act as downstream effectors, responsible for transmitting external signals into intracellular responses[44]. In this study, we proved that the METTL3 silencing-induced DVL2/p-JNK down-regulation could be rescued by intracellular DVL2 overexpression, or a known extracellular DVL2 stimulator FGF-2. This intricate mechanism highlights the crucial role of METTL3 induced m6A modifications that serves similarly as an asymmetric cue in orchestrating expressions of key PCP components, DVL2, and then stimulates downstream p-JNK signaling pathway. Notably, in vivo conditional knockdown of METTL3 in mouse lens results in disrupted alignment of secondary lens fibers, indicating the indispensable role of METTL3 in facilitating polarized fiber alignment, particularly in the recently-differentiated lens fiber derived from LECs. Therefore, we speculate that in lens of high myopia, the differentiated fibers consistently exhibit a polarized behavior where they continuously condense towards the nucleus. This accelerated polarization of the fibers leads to the rapid formation of a more severe nuclear cataract. More importantly, TGF-β1-induced increase of lens fiber compaction in juxtanuclear area and nuclear intensity can be alleviated by METTL3 knockdown. The observed fiber compaction and intensity increase likely arise from secondary effects related to LEC dysfunction in fiber differentiation, rather than direct action on the mature nucleus formed during embryogenesis. Our findings underscore the critical role of METTL3-mediated m6A modifications in regulating DVL2 expression and the PCP signaling pathway in HMC. These insights into molecular mechanisms could help identify potential biomarkers for early detection and prognosis of HMC. Therefore, modulating METTL3 activity or m6A modification levels could open new avenues for preventing or delaying the progression of HMC.

To conclude, our study provides microscopic evidence of highly polarized lens fiber alignment in nuclear cataracts associated with high myopia and revealed TGF-β1-induced METTL3 up-regulation, increased m6A modifications of DVL2 read by IGF2BP3, and stabilized DVL2 that boosts PCP signaling to be the underlying mechanism (Fig. 8). TGF-β1-METTL3-PCP signaling axis is proposed in the promotion of LEC proliferation, migration, and polarity formation in HMC. Each node in this axis holds promise as a potential target for future non-surgical prevention and treatment of early-onset nuclear cataractogenesis for highly myopic patients.

Methods

Patients and samples

Ethics and patients. This study was affiliated with the Shanghai High Myopia Study (NCT03062085) and was reviewed and approved by the Ethics Committee of the Eye & ENT Hospital of Fudan University (Shanghai, China) in accordance with applicable regulations (NO. 2014055). Written informed consents were obtained before surgery from all patients for the use of their clinical data and biosamples including lens epithelia. Patients were not compensated as study participation did not impose any additional burden or inconvenience to their scheduled cataract surgery. Whole-mount human lens samples from age-matched ARC, HMC and clear lens control donor cadavers were collected from Eye Bank at Eye and ENT Hospital of Fudan University. All procedures adhered to the tenets of the Declaration of Helsinki.

Patients who came for cataract surgery in Eye and ENT Hospital of Fudan University from 1 May 2020 to 1 June 2022, and from 1 Feb 2024 to 1 Aug 2024 were consecutively enrolled. Cataract type and severity were graded according to the modified Lens Opacity Classification System III (LOCSIII). The HMC group was recruited according to the following criteria: (1) highly myopic patients with axial lengths of both eyes ≥26.00 mm; (2) developed grade nuclear color (NC) > 3 cataract. The ARC control group was recruited as (1) age-matched non-myopic patients with axial lengths of both eyes between 22.00 and 24.50 mm; (2) developed grade cortex (C) > 3 cataract. Exclusion criteria were other ocular comorbidities such as glaucoma, uveitis, conjunctivitis, etc.; history of ocular surgery or

https://doi.org/10.1038/s41467-025-58995-w

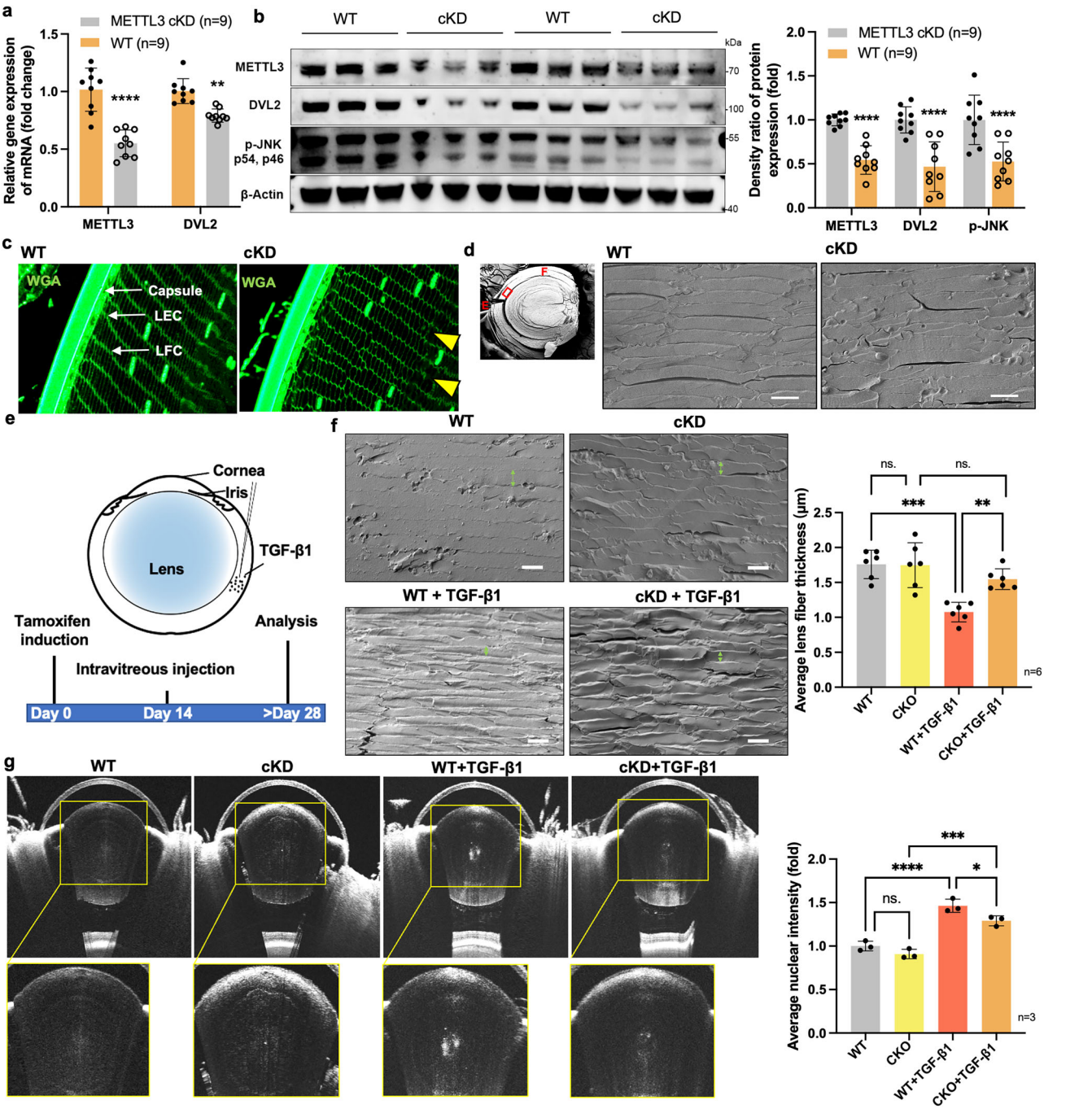

Fig. 7 | Conditional knockdown of METTL3 in mouse lens. a Gene expressions in lens epithelia of *Prox1-CreERT*$^{wt/wt}$;*Mettl3*$^{flox/flox}$ mice (WT) and *Prox1-CreERT*$^{ct2/wt}$;*Mettl3*$^{flox/flox}$ mice (cKD) ($n = 9$, METTL3 $p < 0.0001$, DVL2 $p = 0.0022$). **b** Protein expressions in lens epithelia of WT and cKD mice ($n = 9$, all $p < 0.0001$). **c** Immunostaining of WGA of lens fiber cell membrane in subcapsular areas at the equator of WT and cKD lens. Yellow arrows show the discontinuous cell membrane and disordered alignment. Scale bar: 10 μm. **d** Representative SEM images around subcapsular areas at the equator of WT and cKD lens. Left panel: The primary scam mouse lens half (F front, E equator). Red rectangles showed the ROI of formal SEM scans around subcapsular areas at the equator of lens matrix. Right panel: Representative SEM formal scans of lens fibers. **e** Scheme diagram depicting the timetable of tamoxifen induction and intravitreal injection of active TGF-β1. **f** The representative SEM scans of lens from WT, cKD, and WT or cKD mice after intravitreal injection of TGF-β1. The average lens fiber thickness measured: a random 6 × 6 μm area were chosen to measure the average lens fiber thickness in each lens scans ($n = 6$, WT vs. CKO $p = 0.9997$, WT vs. WT + TGF-β1 $p = 0.0001$, CKO vs. CKO + TGF-β1 $p = 0.3987$, WT + TGF-β1 vs. CKO + TGF-β1 $p = 0.0058$). Scale bar: 2 μm. **g** Swept-source optical coherence tomography scans of lens from WT, cKD, and WT or cKD mice after intravitreal injection of TGF-β1. Yellow rectangles showed the area of partial enlargement view. The mean intensity of the nuclear area was measured by image J. The band density in Western blot was normalized to loading control as a ratio for statistical analysis. Data present are mean ± SD. Level of significance was detected using two-sided two-way ANOVA with Tukey's multiple comparisons test (**a**, **b**, **f**, **g**). n = biological replicates, ns. = not significant, $^{****}p < 0.0001$, $^{***}p < 0.001$, $^{**}p < 0.01$ and $^{*}p < 0.05$.

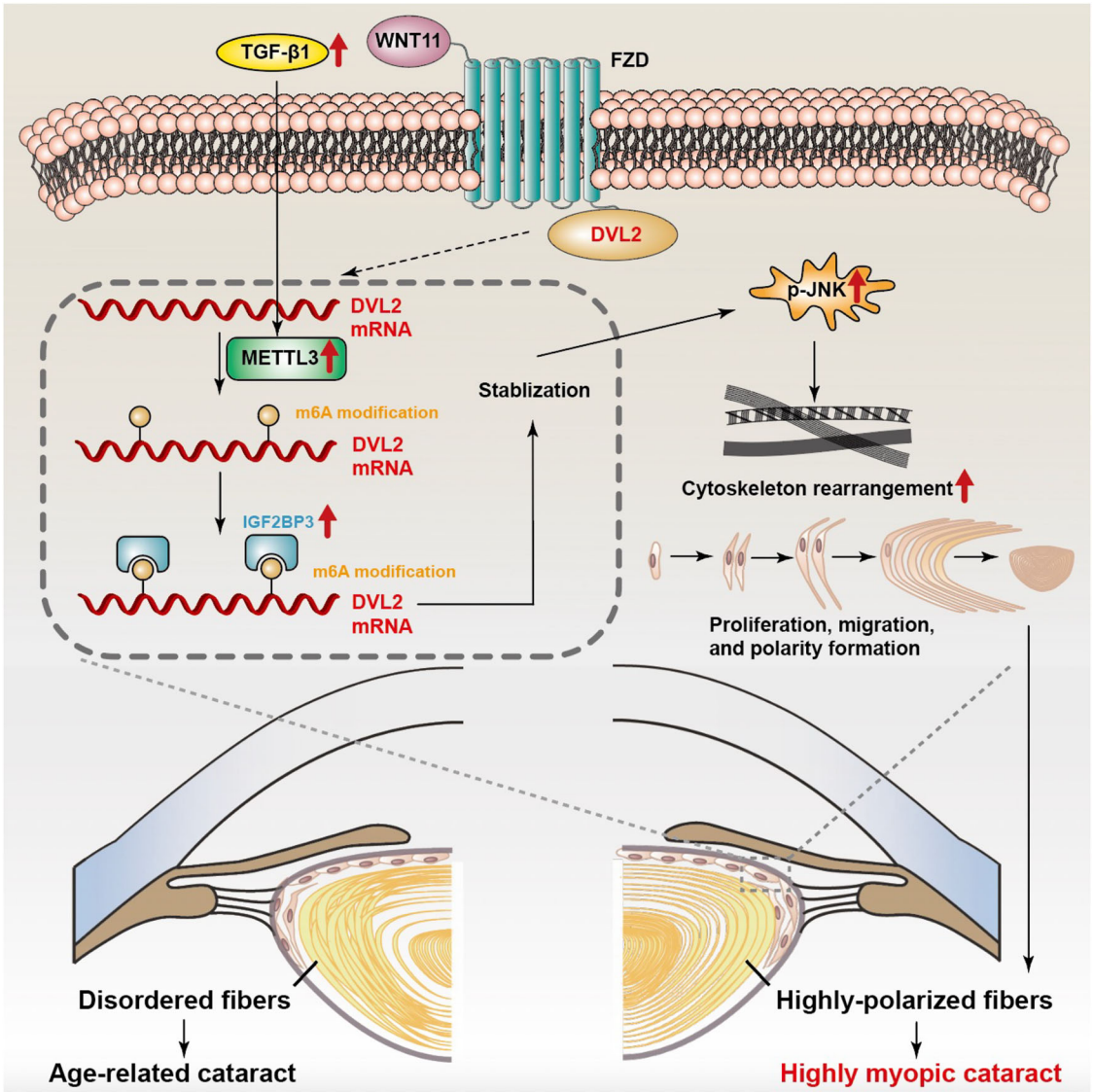

Fig. 8 | The mechanistic scheme of this study. In highly myopic lens, higher TGF-β1 induces increased levels of m6A modifications by up-regulation of METTL3, and m6A modified DVL2 mRNA was then stabilized by m6A reader IGF2BP3. The m6A modification regulates DVL2-dominant PCP signaling pathway, activates downstream p-JNK signaling, and alters cell proliferation, migration, and polarity formation, leading to accelerated nuclear cataract formation in high myopia.

trauma; and systemic diseases such as diabetes, cancer, or malnutrition. The detailed data for included patients and samples were provided in Supplementary Table 1.

Sample acquirement and preservation

Human lens epithelia were collected during standard cataract surgery. Capsulorhexis was conducted before phacoemulsification, during which the anterior lens epithelium with LECs attached on the inner side was peeled off by surgeons and collected (which would be discarded if not for research purpose). Based on the experimental requirement, totally 714 pieces of lens epithelia (357 in HMC group and 357 ARC group, respectively) were collected. Samples were stored at −80 °C until further RNA or protein extractions. For immunofluorescence staining, lens epithelia were fixed with 4% Paraformaldehyde at 4 °C, and handled within 24 h. For primary culture of human LECs, fresh lens epithelia were kept in Dulbecco's Modified Eagle Medium (DMEM) supplemented with 20% fetal bovine serum (FBS), and handled within 24 h.

For qRT-PCR, western blot, and Me-RIP seq, 3–6 pieces of lens epithelia were pooled to reach enough amount of RNA or protein required. For immunofluorescence staining, a single piece of lens epithelium was used as one biological replicate. In primary culture of human LECs, a single piece of lens epithelium was placed in one Petri dish, and used as one biological replicate.

Cell lines

Human LEC cell line SRA 01/04 was purchased from OEbiotech (Shanghai, China), and authentication was done by standard STR profiling analysis.

Animals

Conditional *Mettl3* knockdown C57BL/6J mice were established by the GemPharmatech (Nanjing, China). Mice were housed in specific pathogen-free conditions at 22–24 °C, 50–60% humidity, and a 12-h light/dark cycle with ad libitum access to standard chow and autoclaved water. Mice were kept in individually ventilated cages with bedding and environmental enrichment, and routine handling was performed to minimize stress. Welfare monitoring was conducted daily, assessing body weight, behavior, and general health status, with interventions as needed. Seven-week-old male *Prox1-CreERT*$^{ct2/wt}$;*Mettl3*$^{flox/flox}$ mice received 75 mg kg^{-1} intragastric injection of

10 mg mL^{-1} tamoxifen in corn oil for 7 consecutive days for Cre induction and METTL3 conditional knockdown in lens (cKD)[25]. Age-matched *Prox1-CreERT*$^{wt/wt}$;*Mettl3*$^{flox/flox}$ mice treated with same dose and duration of tamoxifen injections were used at controls (WT). Animals were kept until 6 months old if not for experimental execution for sampling. At the end of the study, mice were euthanized using CO_2 inhalation followed by cervical dislocation. All experimental procedures were approved by the Animal Ethics Committee of Eye and ENT Hospital of Fudan University.

Method details

Cell culture. SRA 01/04 cells were cultured in Dulbecco's Modified Eagle Medium (DMEM) supplemented with 10% FBS. Cells were cultured at 37 °C in a humidified atmosphere with 5% CO_2.

Primary culture was conducted using human lens epithelial samples collected from surgery[35]. Lens epithelia were adhered to the Petri dish and cultured with the LECs side up in the DMEM supplemented with 20% FBS in 37 °C and 5% CO_2, with medium changed every other day.

Measurement of m6A level

Total RNA was extracted from human lens epithelia or SRA 01/04 cells using the RNeasy Micro Kit or the TRIzol reagent as appropriate, following the manufacturer's instructions. The total m6A quantification was conducted using both calorimetric assay and m6A dot blot assay.

An EpiQuik m6A RNA Methylation Quantification Kit was used to detect the total m6A level according to the manufacturer's protocol. Briefly, positive control, negative control, and 200 ng isolated mRNA were added to each well with the capture antibody. Next, the detection antibody was added. After several incubations, the m6A level was quantified calorimetrically at a wavelength of 450 nm.

For m6A dot blot assay, 2 µL RNA samples were loaded onto a nitrocellulose membrane as 100 ng RNA µL^{-1} and UV crosslinked. The membrane blocked with 5% skim milk for 1 h, incubated with primary anti-m6A antibody at 4 °C overnight, then incubated with the secondary antibody for another 1 h at room temperature (RT). After 3 washes in TBST, the membrane was visualized with Immobilon ECL Ultra Western HRP Substrate and the dot blot signals were detected using Fluorescent & Chemiluminescence Gel Imaging System (JS-1070P, Peiqing Science & Technology).

Methylated RNA immunoprecipitation (Me-RIP) assay

The MeRIP assay was conducted by GenSeq™ m6A RNA IP kit according to the manufacturer's instructions. Briefly, isolated mRNA was chemically fragmented into 100 nucleotides or less and immunoprecipitated with anti-m6A antibody or anti-human IgG linked to Magna IP Protein A/G Magnetic Beads. Ten percent fragmented RNA was saved as input. Immunoprecipitated RNA was analyzed through high throughput sequencing (MeRIP seq) or qRT-PCR (MeRIP-qPCR).

Data analyses were then performed[45]: Briefly, Paired-end reads were harvested from Illumina NovaSeq 6000 sequencer, and were quality controlled by Q30. After 3' adapter-trimming and low quality reads removing by cutadapt software (v1.9.3). First, clean reads of input libraries were aligned to reference genome (UCSC HG19) by STAR software. Then clean reads of all libraries were aligned to the reference genome by Hisat2 software (v2.0.4). Methylated sites on mRNAs (peaks) were identified by MACS software. Differentially methylated sites were identified by diffReps. GO and Pathway enrichment analysis were performed by the differentially methylated protein coding genes. The IGV software was used for visualization to observe the abundance of reads at specific locations in the genome of representative sample[46]. MEME software was used for motif analysis.

Transfections

SRA 01/04 cells were seeded into six-well plate overnight and were then transfected with pcDNA3.1-METTL3 with FLAG-tag overexpression plasmid, METTL3 siRNA, or IGF2BP3 siRNA for 48 h. The plasmid, siRNA for human METTL3 (siMETTL3) and IGF2BP3 (siIGF2BP3), and matched negative controls (siNC) were provided by Ribobio (Guangzhou, China). The sequences were shown in Supplementary Table 2. The transfections were performed with Lipofectamine 3000 according to the manufacturer's instructions.

RNA immunoprecipitation (RIP) assays

RIP analysis was performed employing the Magna RIP RNA-Binding Protein Immunoprecipitation Kit in strict accordance with the manufacturer's prescribed protocols. In brief, magnetic beads coated with 5 µg of specific antibodies against IgG, METTL3, or IGF2BP3 were subjected to an overnight incubation with meticulously prepared cellular lysates at 4 °C. Subsequently, the RNA-protein complexes were subjected to six iterative washes and enzymatically treated with proteinase K digestion buffer. The ensuing RNA fraction was ultimately extracted utilizing the phenol-chloroform RNA extraction methods. The quantification of the relative interaction between the METTL3 and IGF2BP3 protein and DVL2 mRNA was achieved through qRT-PCR, with normalization against the input.

RNA stability assays

SRA 01/04 cells were seeded in six-well plates overnight, followed by exposure to actinomycin D (ACTD) at a concentration of 5 µg mL^{-1}. Subsequently, at designated time points of 0-, 2-, 4-, 6-, and 8-h post-treatment, cells were collected and total RNA was extracted utilizing the TRIzol method. The extracted RNA was then subjected to analysis using qRT-PCR. The mRNA expression levels for each experimental group at the specified time intervals were computed and subsequently normalized using GAPDH as a reference. The estimation of mRNA half-life was performed through the utilization of nonlinear regression analysis (one phase decay model).

Cell proliferation and migration assays

To assess cell proliferation, SRA 01/04 cells were seeded in 96-well plates at a density of 1000 cells per well. The 10% CCK-8 was diluted in standard culture media and added to each well, followed by incubation at 37 °C until a visual color conversion was observed. The rates of proliferation were determined at 36 h post-treatment, and the absorbance at 450 nm was measured using a microtiter plate reader (Spectra Rainbow, Tecan) following the protocol recommended by the manufacturer.

Cell migration was assessed using the wound-healing assay. To elaborate, SRA 01/04 cells were cultured in 6-well plates at a density of 50,000 cells per well, utilizing DMEM supplemented with 1% FBS. Subsequently, the cells were subjected to various experimental conditions, and a discrete region of cells was meticulously monitored after 36 h. Images were acquired at both the onset and conclusion of this time period, and wound closure was subsequently quantified via the use of image analysis software (ImageJ).

Quantitative RT-PCR

After extraction of total RNA, cDNA was generated using HiFiScript gDNA removal cDNA Sythesis Kit following the manufacturers' instructions. Gene expression was quantified by qRT-PCR with GAPDH used as an endogenous control gene. The primer used were listed in the Supplementary Table 2.

Western blot analysis

Cell lysates or tissue samples were subjected to treatment with RIPA lysis buffer, which was supplemented with 10 µL mL^{-1} of phosphatase and protease inhibitors, immediately prior to use. The bicinchoninic

acid assay was employed to determine the total protein content, ensuring uniform protein loading onto 4–12% precast mini polyacrylamide gels. Subsequently, the proteins were transferred onto polyvinyl difluoride membranes and then blocked with TBST containing 5% skim milk. Following this, the membranes were incubated with the primary antibody overnight at 4 °C, and then exposed to the secondary antibody for 1 h at RT. The specific antibodies employed in this study can be found in the Supplementary Table 2. Detection of the proteins was achieved using Immobilon ECL Ultra Western HRP Substrate, and visualization was accomplished using a Fluorescent & Chemiluminescence Gel Imaging System.

Immunocytochemistry

Fresh human lens epithelia or paraffin sections of mouse eyeball were fixed in a 4% formaldehyde solution in PBS for a duration of 1.5 h, followed by three consecutive washes in PBS for 10 min each. Subsequently, the samples were permeabilized with 0.3% Triton X-100 for a duration of 15 min, and once again washed three times. To prevent nonspecific binding, a solution containing 0.3% Triton X-100 and 3% BSA was utilized for blocking for a period of 1 h. The primary antibodies were diluted in 1% BSA in PBS and were applied overnight at 4 °C. Following this incubation, three additional washes in PBS were performed, and the secondary antibody, diluted in 1% BSA in PBS, was added for 2 h, while being protected from light and maintaining a humidified atmosphere at RT. To facilitate visualization, the samples were counterstained with DAPI. For the staining of F-actin or WGA, TRITC Phalloidin or FITC conjugate WGA was incubated with DAPI immediately after the blocking step, and this incubation was carried out for 2 h away from light at RT. The samples were examined using fluorescence microscopy (widefield microscope Zeiss Axioplan 2ie; Carl Zeiss Microscopy Ltd, Cambridge, UK). Image quantification was conducted using image analysis software (ImageJ v1.53c). To obtain quantitative data on cell alignment, the 2D Fast Fourier Transform was employed (Supplementary Fig. 1), and this analysis was performed using MATLAB R2021b. The original codes utilized in this study can be available in https://github.com/lingstella/cell-polarity.

Enzyme-linked immunosorbent assay (ELISA)

TGF-β1 concentrations in human lens epithelia or SRA 01/04 cells were detected by a human/mouse/rat TGF-β1 ELISA kit. Phospho-JNK and total-JNK concentrations in human lens epithelia or SRA 01/04 cells were detected by Phospho-SAPK/JNK (Thr183/Tyr185) Sandwich ELISA Kit and Total SAPK/JNK Sandwich ELISA Kit.

Freeze-fracture electron microscope

Whole-mount human lens samples from age-matched ARC, HMC and clear lens control donor cadavers were used within 72 hours of death. Whole-mount mouse lens samples were dissected from cKD and WT eyes. Fresh lens samples were fixes in 2% formaldehyde-2.5% glutaraldehyde in 100 nM sodium cacodylate buffer (pH 7.2) for 7 days at 4 °C. They were then washed in sodium cacodylate buffer at RT and then cryoprotected with 25% glycerol in 100 nM sodium cacodylate buffer overnight at 4 °C and processed for freeze-fracture in liquid nitrogen, to better present cross-fractured lens fibers[32,47]. Each lens was properly orientated and fractured with a sharp blade to expose the longitudinal configuration of narrow-side fibers at the anterior, equatorial and posterior regions. Lens halves then refixed for 2 h with 1% osmium tetroxide, and then were dehydrated using a graded ethanol series (30%, 50%, 75%, 80%, 95%) at 4 °C with each incubation step lasting 30 min. The series was completed by fully dehydrating the samples in 100% ethanol (three times, 30 min for each) at 4 °C. The lens halves were then dried in a critical point dryer (EM CPD300, Leica, German), after which the samples were prepared under a microscope to ensure that the fractured surfaces were facing upward. Finally, samples were treated with a turbomolecular pumped coater (Q150T ES, Quorum, England). The prepared samples were then scanned using a field-emission SEM instrument (GeminiSEM 300, Carl Zeiss AG, German).

Intravitreal injection

Intravitreal injection is a proven method that effectively and safely delivers drug to influence LECs of animal lens without inducing unwanted damage[48,49]. WT and cKD Mice were anesthetized by 1% pentobarbital sodium, and pupils were dilated with 0.5% tropicamide and 0.5% phenylephrine. A step incision in the pars plana region of the sclera was made using a 30-gauge needle. Subsequently, a microliter syringe equipped with a 33-gauge blunt needle (Hamilton Bonaduz AG, Bonaduz, Switzerland) was carefully inserted into the vitreous cavity at the 6 o'clock position, ensuring an injection angle of 45° for the right eye. Under the guidance of a surgical microscope (Leica Microsystems. Ltd.,Wetzlar, Germany), 200 ng of TGF-β1 was gently delivered into the eye.

Swept-source optical coherence tomography

A swept-source OCT system (YG-100K Yalkaid, TowardPi Medical Technology, Beijing, China) was used to obtain anterior segment OCT images of cataract patients, and whole eyeball OCT images for mice. All measurements were carried out with mydriasis eye drops containing 0.5% tropicamide and 0.5% phenylephrine. For mice, procedures were done after general anesthesia by 1% pentobarbital sodium.

Quantification and statistical analysis

Sample size calculation was performed using G*Power Software 3.1 for t-test, with a desired significance level of 5% and a test power of 0.95. Samples with missing key variables or quality control issues were excluded following pre-established exclusion criteria. Investigators were blinded to group allocation during data analysis to minimize bias. Statistical analyses were performed using SPSS 22.0 or GraphPad Prism 9 software. Data are expressed as the mean and standard deviation of at least three independent experiments. Mann-Whitney *U* test or unpaired Student's *t*-test was performed to compare the variables of the two sample groups where appropriate. One-way analysis of variance (ANOVA) test were used to compare the differences among multiple groups. The Pearson correlation coefficient was used to evaluate the correlation between nuclei intensity and TGF-β1 concentrations. A p value of <0.05 was considered significant.

Reporting summary

Further information on research design is available in the Nature Portfolio Reporting Summary linked to this article.

Data availability

Data supporting the findings of this study are available in the article and its Supplementary information. Source data are provided as Source Data file and may be obtained from the corresponding authors upon request. The sequencing data reported in this paper are deposited in NCBI Gene Expression Omnibus (GEO) database with accession number GEO: GSE244037. Source data are provided with this paper.

Code availability

All original codes of the analyses are available at https://github.com/lingstella/cell-polarity.

References

1. Holden, B. A. et al. Global prevalence of myopia and high myopia and temporal trends from 2000 through 2050. *Ophthalmology* **123**, 1036–1042 (2016).
2. Morgan, I. G. et al. The epidemics of myopia: aetiology and prevention. *Prog. Retin. Eye Res.* **62**, 134–149 (2018).

3. Praveen, M. R. et al. A study to explore the risk factors for the early onset of cataract in India. *Eye* **24**, 686–694 (2010).
4. Saw, S. M., Gazzard, G., Shih-Yen, E. C. & Chua, W. H. Myopia and associated pathological complications. *Ophthalmic Physiol. Opt.* **25**, 381–391 (2005).
5. Zhu, X. J. et al. Epigenetic regulation of αA-crystallin in high myopia-induced dark nuclear cataract. *PLoS ONE* **8**, e81900 (2013).
6. Praveen, M. R., Vasavada, A. R., Jani, U. D., Trivedi, R. H. & Choudhary, P. K. Prevalence of cataract type in relation to axial length in subjects with high myopia and emmetropia in an Indian population. *Am. J. Ophthalmol.* **145**, 176–181 (2008).
7. Zhu, X., Li, D., Du, Y., He, W. & Lu, Y. DNA hypermethylation-mediated downregulation of antioxidant genes contributes to the early onset of cataracts in highly myopic eyes. *Redox Biol.* **19**, 179–189 (2018).
8. Zhu, X. et al. Proinflammatory status in the aqueous humor of high myopic cataract eyes. *Exp. Eye Res.* **142**, 13–18 (2016).
9. Zhu, X. et al. Aberrant TGF-beta1 signaling activation by MAF underlies pathological lens growth in high myopia. *Nat. Commun.* **12**, 2102 (2021).
10. Zhao, L. et al. Lanosterol reverses protein aggregation in cataracts. *Nature* **523**, 607–611 (2015).
11. Chen, Y., Stump, R. J., Lovicu, F. J. & McAvoy, J. W. A role for Wnt/planar cell polarity signaling during lens fiber cell differentiation? *Semin. Cell Dev. Biol.* **17**, 712–725 (2006).
12. Dawes, L. J., Sugiyama, Y., Tanedo, A. S., Lovicu, F. J. & McAvoy, J. W. Wnt-frizzled signaling is part of an FGF-induced cascade that promotes lens fiber differentiation. *Investig. Ophthalmol. Vis. Sci.* **54**, 1582–1590 (2013).
13. Han, C. et al. Wnt5a contributes to the differentiation of human embryonic stem cells into lentoid bodies through the noncanonical Wnt/JNK signaling pathway. *Investig. Ophthalmol. Vis. Sci.* **59**, 3449–3460 (2018).
14. Chen, Y., Stump, R. J., Lovicu, F. J., Shimono, A. & McAvoy, J. W. Wnt signaling is required for organization of the lens fiber cell cytoskeleton and development of lens three-dimensional architecture. *Dev. Biol.* **324**, 161–176 (2008).
15. Kim H., Jang S. & Lee Y. S. The m6A(m)-independent role of FTO in regulating WNT signaling pathways. *Life Sci. Alliance.* **5**, e202101250 (2022).
16. Ma, X. et al. METTL3 attenuates proliferative vitreoretinopathy and epithelial-mesenchymal transition of retinal pigment epithelial cells via wnt/β-catenin pathway. *J. Cell Mol. Med* **25**, 4220–4234 (2021).
17. Li, T. et al. Silencing of METTL3 attenuates cardiac fibrosis induced by myocardial infarction via inhibiting the activation of cardiac fibroblasts. *FASEB J.* **35**, e21162 (2021).
18. Liu, Y., Gu, C., Li, X., Wang, T. & Yu, L. Involvement of METTL3/m(6)Adenosine and TGFβ/Smad3 signaling on Tenon's fibroblasts and in a rabbit model of glaucoma surgery. *J. Mol. Histol.* **52**, 1129–1144 (2021).
19. Zhao, X. et al. Alterations of the m(6)A methylation induced by TGF-β2 in ARPE-19 cells.*Front. Biosci.* **28**, 148 (2023).
20. Wu, Z. et al. METTL3 counteracts premature aging via m6A-dependent stabilization of MIS12 mRNA. *Nucleic Acids Res.* **48**, 11083–11096 (2022).
21. Yang, J., Liu, J., Zhao, S. & Tian, F. N(6)-methyladenosine METTl3 modulates the proliferation and apoptosis of lens epithelial cells in diabetic cataract. *Mol. Ther. Nucleic Acids* **20**, 111–116 (2020).
22. Huang, H. et al. Recognition of RNA N(6)-methyladenosine by IGF2BP proteins enhances mRNA stability and translation. *Nat. Cell Biol.* **20**, 285–295 (2018).
23. Wang, X. et al. N6-methyladenosine-dependent regulation of messenger RNA stability. *Nature* **505**, 117–120 (2014).
24. Bianchi, R. et al. A transgenic Prox1-Cre-tdTomato reporter mouse for lymphatic vessel research. *PLoS ONE* **10**, e0122976 (2015).
25. Dawes, L. J. et al. Interactions between lens epithelial and fiber cells reveal an intrinsic self-assembly mechanism. *Dev. Biol.* **385**, 291–303 (2014).
26. Das, S. J., Lovicu, F. J. & Collinson, E. J. Nox4 plays a role in TGF-β-dependent lens epithelial to mesenchymal transition. *Investig. Ophthalmol. Vis. Sci.* **57**, 3665–3673 (2016).
27. Periyasamy, P. & Shinohara, T. Age-related cataracts: role of unfolded protein response, Ca(2+) mobilization, epigenetic DNA modifications, and loss of Nrf2/Keap1 dependent cytoprotection. *Prog. Retin. Eye Res.* **60**, 1–19 (2017).
28. Zhu, X. J. et al. Racemization at the Asp 58 residue in alphaA-crystallin from the lens of high myopic cataract patients. *J. Cell Mol. Med.* **22**, 1118–1126 (2018).
29. Lovicu, F. J., McAvoy, J. W. & de Iongh, R. U. Understanding the role of growth factors in embryonic development: insights from the lens. *Philos. Trans. R. Soc. Lond. B Biol. Sci.* **366**, 1204–1218 (2011).
30. Bassnett, S. & Šikić, H. The lens growth process. *Prog. Retin. Eye Res.* **60**, 181–200 (2017).
31. Al-Ghoul, K. J. et al. Structural evidence of human nuclear fiber compaction as a function of ageing and cataractogenesis. *Exp. Eye Res.* **72**, 199–214 (2001).
32. Gu, S. et al. Connexin 50 and AQP0 are essential in maintaining organization and integrity of lens fibers. *Investig. Ophthalmol. Vis. Sci.* **60**, 4021–4032 (2019).
33. Kalicharan, D., Jongebloed, W. L. & Worst, J. G. Lensfibre degeneration at cataract lenses. A LM, SEM and TEM investigation. *Doc. Ophthalmol.* **85**, 77–85 (1993).
34. Pelton, R. W., Saxena, B., Jones, M., Moses, H. L. & Gold, L. I. Immunohistochemical localization of TGF beta 1, TGF beta 2, and TGF beta 3 in the mouse embryo: expression patterns suggest multiple roles during embryonic development. *J. Cell Biol.* **115**, 1091–1105 (1991).
35. West-Mays, J. A., Pino, G. & Lovicu, F. J. Development and use of the lens epithelial explant system to study lens differentiation and cataractogenesis. *Prog. Retin. Eye Res.* **29**, 135–143 (2010).
36. Roundtree, I. A., Evans, M. E., Pan, T. & He, C. Dynamic RNA modifications in gene expression regulation. *Cell* **169**, 1187–1200 (2017).
37. Meyer, K. D. & Jaffrey, S. R. The dynamic epitranscriptome: N6-methyladenosine and gene expression control. *Nat. Rev. Mol. Cell Biol.* **15**, 313–326 (2014).
38. Yao, M. D. et al. Role of METTL3-dependent N(6)-methyladenosine mRNA modification in the promotion of angiogenesis. *Mol. Ther.* **28**, 2191–2202 (2020).
39. Liu, K. et al. Altered ubiquitin causes perturbed calcium homeostasis, hyperactivation of calpain, dysregulated differentiation, and cataract. *Proc. Natl. Acad. Sci. USA* **112**, 1071–1076 (2015).
40. Kaucká, M. et al. The planar cell polarity pathway drives pathogenesis of chronic lymphocytic leukemia by the regulation of B-lymphocyte migration. *Cancer Res.* **73**, 1491–1501 (2013).
41. Guo, Z. et al. METTL3-IGF2BP3-axis mediates the proliferation and migration of pancreatic cancer by regulating spermine synthase m6A modification. *Front. Oncol.* **12**, 962204 (2022).
42. Sun, C. Y., Cao, D., Du, B. B., Chen, C. W. & Liu, D. The role of Insulin-like growth factor 2 mRNA-binding proteins (IGF2BPs) as m(6)A readers in cancer. *Int J. Biol. Sci.* **18**, 2744–2758 (2022).
43. Wan, W. et al. METTL3/IGF2BP3 axis inhibits tumor immune surveillance by upregulating N(6)-methyladenosine modification of PD-L1 mRNA in breast cancer. *Mol. Cancer* **21**, 60 (2022).
44. Xu, Y. et al. Loss of polarity protein AF6 promotes pancreatic cancer metastasis by inducing Snail expression. *Nat. Commun.* **6**, 7184 (2015).
45. Meyer, K. D. et al. Comprehensive analysis of mRNA methylation reveals enrichment in 3′ UTRs and near stop codons. *Cell* **149**, 1635–1646 (2012).

46. Thorvaldsdóttir, H., Robinson, J. T. & Mesirov, J. P. Integrative Genomics Viewer (IGV): high-performance genomics data visualization and exploration. *Brief. Bioinform.* **14**, 178–192 (2013).
47. Lo, W. K. et al. Aquaporin-0 targets interlocking domains to control the integrity and transparency of the eye lens. *Investig. Ophthalmol. Vis. Sci.* **55**, 1202–1212 (2014).
48. Nagai, N. et al. The Intravitreal injection of lanosterol nanoparticles rescues lens structure collapse at an early stage in shumiya cataract rats. *Int. J. Mol. Sci.* **21**, 1048 (2020).
49. Liang, Y., Lan, T., Gan, Q. & Liang, H. Successful transduction of target gene mediated by adeno-associated virus 2 into lens epithelial cells in rats. *J. Virol. Methods* **321**, 114792 (2020).

Acknowledgements

This study was supported by research grants from the National Natural Science Foundation of China (82122017, 82271069, 81870642, and 81470613 [X.Z.]; 82371040, 81970780, and 81670835 [Y.L.]), Science and Technology Innovation Action Plan of Shanghai Science and Technology Commission (23Y11909800 [X.Z.]), Outstanding Youth Medical Talents of Shanghai "Rising Stars of Medical Talents" Youth Development Program (X.Z.), Shanghai Municipal Health Commission Project (2024ZZ1025 and 20244Z0015 [X.Z.]). We would like to thank Dr Yu Kong and Xu Wang (Electron Microscopy Facilities of Center for Excellence in Brain Science and Technology, Chinese Academy of Science) for assistance with SEM sample preparation and SEM images analyze work.

Author contributions

L.W. and X.Z. conceptualized and designed this study. L.W. and Y.D. performed and analyzed most of the experiments. S.G. performed and executed the bioinformatic analyses and supported the animal experiments. D.L. supported MERIP-seq analysis. W.H., K.Z., and Y.L. supported human sample collection. L.W. and Y.D. wrote the draft manuscript, and all authors reviewed the manuscript.

Competing interests

The authors declare no competing interests.

Additional information

Supplementary information The online version contains supplementary material available at https://doi.org/10.1038/s41467-025-58995-w.

Correspondence and requests for materials should be addressed to Xiangjia Zhu.

Peer review information *Nature Communications* thanks Hua-Bing Li, and the other, anonymous, reviewer(s) for their contribution to the peer review of this work. A peer review file is available.